

Semantic Image Manipulation with Background-guided Internal Learning

Zhongping Zhang¹, Huiwen He¹, Bryan A. Plummer¹,
Zhenyu Liao², and Huayan Wang³

¹ Boston University, {zpzhang, huiwenhe, bplum}@bu.edu

² Amazon, {zyliao}@amazon.com

³ Kuaishou AI Lab, {wanghy514}@gmail.com

Abstract. Image manipulation has attracted a lot of interest due to its wide range of applications. Prior work modifies images either from low-level manipulation, such as image inpainting or through manual edits via paintbrushes and scribbles, or from high-level manipulation, employing deep generative networks to output an image conditioned on high-level semantic input. In this study, we propose Semantic Image Manipulation with Background-guided Internal Learning (SIMBIL), which combines high-level and low-level manipulation. Specifically, users can edit an image at the semantic level by applying changes on a scene graph. Then our model manipulates the image at the pixel level according to the modified scene graph. There are two major advantages of our approach. First, high-level manipulation of scene graphs requires less manual effort from the user compared to manipulating raw image pixels. Second, our low-level internal learning approach is scalable to images of various sizes without reliance on external visual datasets for training. We outperform the state-of-the-art in a quantitative and qualitative evaluation on the CLEVR and Visual Genome datasets. Experiments show 8 points improvement on FID scores (CLEVR) and 27% improvement on user evaluation (Visual Genome), demonstrating the effectiveness of our approach.

Keywords: semantic image manipulation, internal learning, scene graph editing

1 Introduction

Image manipulation modifies the content of an image according to user guidance. The task can be solved in two primary ways: low-level manipulation on raw images and high-level manipulation on image semantics. Low-level manipulation spans image inpainting [43, 54], colorization [49], object removal [35], style transfer [9], image extension [36], etc. Low-level manipulation methods do not need to understand the semantic meanings of an image. In contrast, high-level manipulation often uses deep generative networks conditioned on user inputs like semantic maps and language descriptions to identify the desired modifications. Most prior work for high-level image manipulation are object-centric,

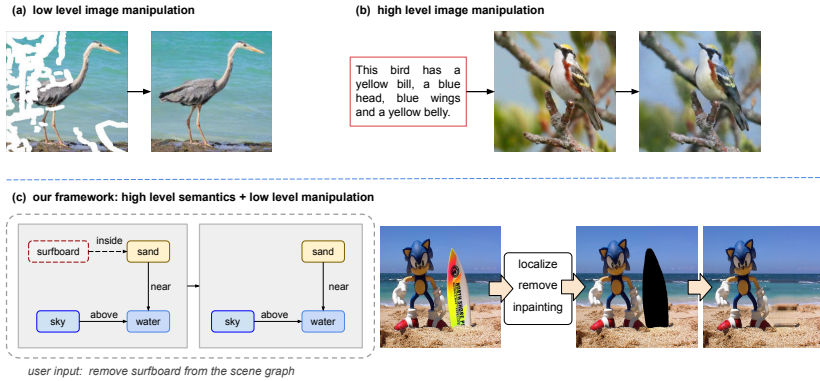


Fig. 1. Prior work of image manipulation is either at a low-level, shown in (a), or high-level, shown in (b). High-level manipulation based on deep generative models, requires less human effort than low-level manipulation. However, generative models rely on external training data and can lose important details and attributes from the original images. Thus, in our work, shown in (c), we address these issues by connecting high-level semantics with low-level manipulation, where the semantic level information is encoded by scene graphs and an RNN-based position prediction model. Then the low-level manipulation, background-guided internal learning, is done according to the processed information.

such as human face transfer [4, 17, 22, 53] and object appearance or attribute modification [23, 26]. Recently, approaches modifying the entire scenes by instance maps [39], language descriptions [7] or scene graphs [6] are also proposed. Although high-level manipulation requires less manual effort from users, deep generative networks for high-level manipulation have two drawbacks. First, the output images are limited by a fixed size, which often only supports outputting low resolution images due to GPU memory requirements [6]. Second, generative models may result in the loss of attributes and details of the original images [1].

Ideally, a good image manipulation method should satisfy the following requirements: (1) provide maximum convenience to users; for example, manipulating images by scene graphs or language description is more convenient than manually segmenting, replacing, or removing the target object, (2) preserve the textures and details of the original image in appropriate areas, (3) correctly modify the target region of the image according to user instructions, (4) ability to generalize across input images without relying on specific external datasets.

Motivated by these requirements, we propose a Semantic Image Manipulation framework with Background-guided Internal Learning (SIMBIL). SIMBIL combines high-level image semantics with low-level manipulation. Figure 1 illustrates the difference between SIMBIL and prior work by an object removal example. Figure 2 presents the overall structure of SIMBIL. First, the target object is determined by the scene graph of an image. The users are able to edit the nodes and edges of scene graphs for four operations, object removal, ob-

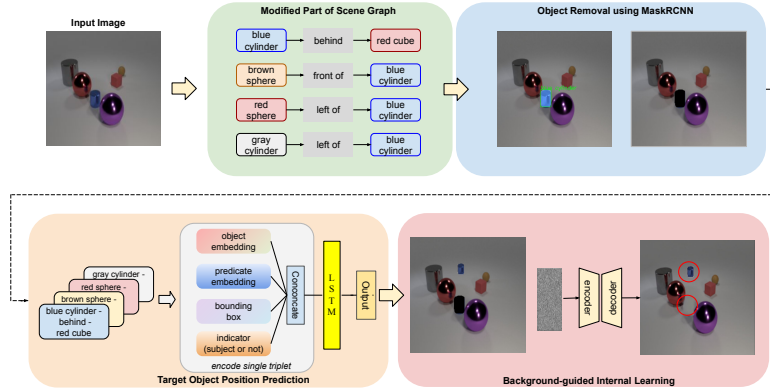


Fig. 2. SIMBIL overview. Given an input image and its modified scene graph, our approach consists of three modules in sequence: (1) Object Removal Module: segmenting and removing the target object from the original region; (2) Position Prediction Module: predicting the new position of the target object by encoding the modified triplets of the scene graph; (3) Internal Learning Module: leveraging the average value of the background pixels around the target object to guide the inpainting results.

object replacement, semantic relationship change, and object addition. Then we use a segmentation network, Mask R-CNN [12], to outline and remove the target object. In addition, we develop a Recurrent Neural Networks (RNN)-based model to encode the semantic relationship modification between the objects. Finally, we improve the deep image prior (DIP) [37] framework by utilizing the background pixels as a constraint and propose the background-guided internal learning method.

In summary, the contributions of this paper are:

- We propose a semantic image manipulation framework (SIMBIL) to combine high-level semantics with low-level image manipulation, reducing manual effort and alleviating the issues caused by deep generative networks of prior work. Notably, compared to existing manipulation methods using scene graphs [6], SIMBIL can generate higher resolution images while accurately preserving the original details of the input images.
- We develop a background-guided internal learning algorithm based on DIP [37] for image inpainting, which utilizes the average value of the background pixels around the missing part as guidance as opposed to only relying on the implicit prior captured by the neural network parameterization, boosting performance.
- Quantitative and qualitative experiments on CLEVR [18] and Visual Genome [21] demonstrate SIMBIL outperforms the state-of-the-art.
- Extensive experiments on high resolution images demonstrate SIMBIL’s flexibility and scalability.

2 Related Work

Image Manipulation can be seen as a special case of image synthesis. Many studies based on image synthesis focus on object-centric scenarios, *e.g.*, editing human face [4, 17, 22, 43, 53], text-guided attribute manipulation [23], changing object categories [26], manually editing with paintbrush and scribbles [2, 56].

The most common framework for scene-level manipulation is image inpainting, a type of low-level manipulation. Prior work conditioned on user-specified templates [17, 54], latent image features [1], or object removal [35]. Recently there has been some work on high-level manipulation modifying the entire scenes [6, 7, 39]. Wang *et al.* [39] conditioned on instance maps to synthesis high-resolution images, enabling to interactively manipulate images by modifying the instance maps. El-Nouby *et al.* [7] divided text-to-image generation into several steps; each step can be considered as an object addition task via language descriptions. Dhano *et al.* [6] proposed a scene graph-based approach that could not only make modifications to visual objects, but also change the semantic relationships between objects in a single image. Unlike these methods primarily based on generative networks, SIMBIL adopts an automatic “photoshop” mechanism, directly manipulating raw image pixels. Our method is applicable to different input images while preserving the original image details well.

Internal Learning. While external learning trains a model on external datasets, internal learning methods such as Deep Image Prior [37] use a generator network trained on a single image to address tasks like image denoising, inpainting, and super-resolution. Internal learning is not limited to image inverse problems [11, 51, 52], but has other applications including video motion transfer [3], video inpainting [47], and semantic photo manipulation [1]. Gandelsman *et al.* [8] also used coupled DIPs to unsupervised image decomposition. In this paper, we introduce a background-guided mechanism based on DIP, which leverages the background pixels as more accurate guidance than the implicit prior used by the original authors for the missing region of an image.

Scene Graphs and Visual Relationship Detection. Scene graphs [19] describe the objects, attributes of objects, and relationships between objects in an image, and methods that generate them can be divided into two categories: Convolutional Neural Network (CNN)-based methods [24, 25, 33, 42] and Recurrent Neural Networks (RNN)-based methods [13, 41, 45]. At a high level, scene graph construction combines object/entity detection [32, 34] and detecting their visual relationships [5, 29, 31].

In our paper, users can apply changes to the relationships between objects to realize image manipulation. A relevant task is visual entity localization according to visual relationships. Krishna *et al.* [20] introduce an iterative model to localize the entities in the referring relationship. Plummer *et al.* [31] combine linguistic cues with learned weights for phrase localization. In our project, the main difference is that the target object is invisible in the image. Therefore, we propose an RNN-based method to automatically predict a plausible position

for the target object according to the existing information from the image and `<subject-predicate-object>` triplets.

3 SIMBIL

Given an input image I and its corresponding scene graph G , users can apply changes on G . Our task is to perform semantic manipulation according to the user-modified scene graph \tilde{G} and the original input image I . In practice, G can be obtained by scene graph generation methods [13, 24, 33, 41, 45]. Following [6], we use ground truth scene graphs in our experiments so the accuracy of current methods is not a factor in evaluating our approach. Figure 2 provides an overview of our framework. We introduce four kinds of modifications on scene graphs in Section 3.1. In Section 3.2, we discuss the details of our position prediction model. The background-guided internal learning algorithm is then presented in Section 3.3. Finally, we summarize the overall learning strategy in Section 3.4.

3.1 Modifications on Scene Graphs

Following [6], we perform four tasks of semantic manipulation in total: object addition, object replacement, relationship change, and object removal⁴. These manipulations are mainly reflected on the nodes and edges of scene graphs. Take the blue cylinder in Figure 2 as an example, (1) Object Addition: adding a new object (node) and its corresponding relationships (edges) with other objects on the scene graph; (2) Object Replacement: replacing the node which represents `<blue cylinder>` to another object; (3) Relationship Change: changing one spatial relationship of blue cylinder (edge) from `<blue cylinder-front of-red cube>` to `<blue cylinder-behind-red cube>`. The other relationships of the blue cylinder can be changed similarly; (4) Object Removal: deleting the node of `<blue cylinder>` and its corresponding edges.

Given the modified scene graph \tilde{G} , we extract the category and bounding box of the target object and obtain its mask with Mask R-CNN [12], but any segmentation method could be used.

3.2 Position Prediction

We introduce a Position prediction module to support the object addition and relationship change (object reposition) tasks. Unlike relationship detection [21], which identifies relationships between a visible reference and target object in a scene, our goal is to determine where to place the target object given the reference object and its semantic relationship to the target object. In addition, multiple relationships may need to be encoded as the target object may have relationships with multiple objects in the scene. Inspired by RNN-based methods on scene graph generation [13, 45], we develop an LSTM-based model that encodes all the triplets of the modified scene graph.

⁴ Four operations on CLEVR [18], three operations on Visual Genome [21]: object replacement, relationship change, and object removal

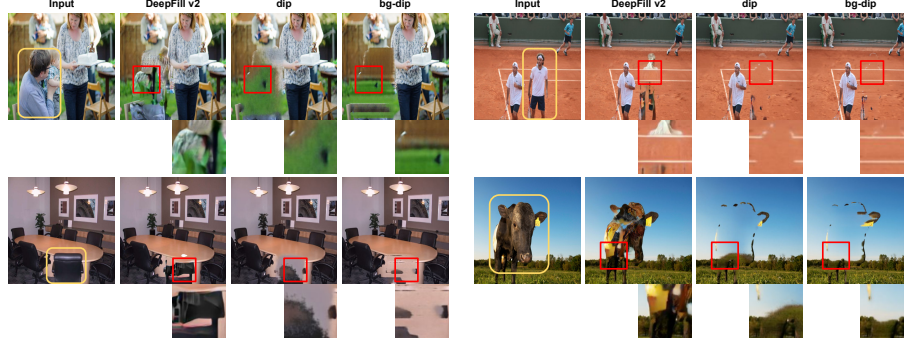


Fig. 3. Comparison of external learning (DeepFill v2) and internal learning (dip & bg-dip) on Visual Genome, where bg-dip denotes our background-guided internal learning.

We define the categories of the entities (subject & object) in images as $O = \{o_1, \dots, o_n\}$, their corresponding bounding boxes as $B = \{b_1, \dots, b_n\}$, and the relationships (predicates) between entities as $R = \{r_1, \dots, r_m\}$. Given the modified scene graph \tilde{G} and the target object o in an image, the triplets of the target object are referred as $\mathbf{y} = \{y_1, \dots, y_T\}$. For $t \in \{1, \dots, T\}$, y_t is a triplet in $\langle s - p - o \rangle$ format, where $s, o \in O$ and $p \in R$. For each triplet y_t , we devise two embedding layers that obtain the object embedding V_s , V_o and predicate embedding V_p separately. We also introduce a binary indicator I to indicate whether the target object is subject or object in y_t . Suppose the reference object corresponds to “subject” and the target object corresponds to “object”, we also consider the position of reference object b_s as part of the input to our model. The concatenation of these features are encoded by a LSTM model. Specifically, it can be expressed as:

$$x_t = \text{concat}\{V_s, V_o, V_p, b_s, I\} \quad (1)$$

$$h_t = \text{LSTM}(x_t, h_{t-1}) \quad (2)$$

where h_t is the hidden state of LSTM at triplet y_t . It needs to mention that in CLEVR [18] dataset, we get rid of the V_s and V_o because the predicates in CLEVR dataset only cover the spatial relationships. In this case, the class labels of the objects should not influence the final result.

h_T is followed by fully connected layers to predict the target object position. We crop the final output to range (0~1) since the image size is normalized. Mean square error (MSE) loss is applied to optimize the parameters.

3.3 Background-guided Internal Learning

Our internal learning approach, SIMBIL, has two advantages over external learning methods [30, 44, 46]. First, external learning methods rely on the training



Fig. 4. Left: deep image prior; Right: our background-guided internal learning.

data that consists of image pairs before and after inpainting. Thus, an inpainting model for CLEVR and Visual Genome needs to be trained separately and is not applicable to different input images. Second, even if we use free-form image inpainting datasets like [44], external learning methods tend to repair rather than remove objects. This is because these models use the ground truth image instead of the modified image as supervision (*i.e.*, Visual Genome lacks before and after editing image pairs). In Figure 3, we compare the internal learning approaches with the external learning method DeepFill v2 [44] which is pre-trained on Places2 [55]. As shown in these examples, when DeepFill v2 is applied to Visual Genome [21] it attempts to repair the object according to the boundary information. Thus, we adopt an internal learning-based method for inpainting.

Given an image x_0 and a binary mask m , the input to image inpainting is $x_0 \odot m$, where m defines the known areas of image x_0 (1 for the known regions and 0 otherwise) and \odot denotes Hadamard’s product. The standard image inversion problem can be formulated by

$$x^* = \underset{x}{\operatorname{argmin}} E(x; x_0) + R(x) \quad (3)$$

where $E(x; x_0)$ is a task-dependent data term and $R(x)$ is the regularization term. For deep image prior (DIP) [37], the regularization term $R(x)$ is replaced by the implicit prior from the neural network parametrization. Specifically, the input of the generative neural network is a noise map z that has one channel and shares the same spatial size as image x_0 . The network parameters are updated to minimize $E(x; x_0)$. In terms of image inpainting, $E(x; x_0)$ satisfies

$$E(x; x_0) = ||(x - x_0) \odot m||^2 \quad (4)$$

where x is the output of the generative model. Note that our “missing” regions are determined by a segmentation model, *i.e.*, the boundary of the hole might not be accurate. Thus, the generative network may be given a noisy input, resulting in incorrect predictions by prior work like DIP. In addition, the object to remove can be large, in which case the relative performance of DIP is worse [37, 47].

We address the aforementioned issue with noisy inputs in two ways. First, we use mask dilation to alleviate the misinformation of the boundary. Second, we

use the background pixels around the hole as guidance to the model. Specifically, suppose a consistent background is divided into two parts; the distributions of each part should still be consistent with the other. As shown in Figure 4, the segmentation of the target car is the missing region of the original image. Then the background pixels within the red bounding box are extracted from the image. We constrain the average of the missing region by the average of the specified background region. Denote the average value of background pixels as B , $B \in \mathbb{R}^3$. our new objective function is

$$E(x; x_0) = ||(x - x_0) \odot m||^2 + \lambda \frac{1}{C} ||average(x \odot (1 - m)) - B||^2 \quad (5)$$

where C represents the number of image channels, and λ is the hyper-parameter to control the two loss terms. In practice, the second loss term can be further divided into sub-terms, for example, constraining the average row by row.

3.4 Overall Learning Strategy

There are three components in our framework, which are Mask R-CNN, position prediction model, and background-guided internal learning. Mask R-CNN is applied in two cases (1) removing the target object from the original position (2) searching relevant objects (from the current image or query images) given the object category, which is mainly for addition, reposition, and replace tasks. The position prediction model is designed for addition and reposition tasks. To train this model, we extract modified triplets, bounding boxes of reference objects, and target objects to construct a dataset. Take CLEVR as an example; we extract 6688 images from the training set to construct the training data, then the 818 images in the validation set are used to evaluate the performance of the model. The target object is pasted according to the predicted position of the model. After this step, remember we still need to address the missing region (“hole”). The background-guided internal learning is employed here to get the final output.

4 Experiments

4.1 Datasets and Experiment Settings

Datasets. We evaluate on CLEVR [18] and Visual Genome [21]. CLEVR is a synthetic dataset that contains ground truth pairs for image editing. For a fair comparison, we use the test set provided by [6]. Visual Genome, on the other hand, lacks before and after image editing pairs. Therefore, we leverage human evaluation to estimate the correctness of manipulation. We also introduce a novel way to measure the quality of manipulated images, *i.e.*, a forensic detection model is applied to detect various image inpainting manipulations. Similar to the adversarial mechanism [10], higher-quality images are supposed to be more

Method	All pixels				RoI only	
	MAE ↓	SSIM ↑	LPIPS ↓	FID ↓	MAE ↓	SSIM ↑
Image Resolution	64 × 64					
SIMSG-CRN [6]	7.83	96.16	0.036	6.32	27.78	77.65
SIMSG-SPADE [6]	5.47	96.51	0.035	4.73	28.66	77.43
SIMBIL (Position+DIP)	1.67	97.16	0.036	6.51	22.18	71.26
SIMBIL (Position+DIP+guide)	1.55	97.31	0.032	7.57	16.80	76.26
SIMBIL (Position+DIP+guide+dilation)	1.53	97.49	0.029	6.08	16.33	78.98
Image Resolution	128 × 128					
SIMSG-CRN [6]	14.54	95.99	0.071	9.78	27.72	75.54
SIMSG-SPADE [6]	8.06	97.40	0.061	4.66	23.70	77.09
SIMBIL (Position+DIP)	1.75	97.85	0.063	5.97	24.03	70.32
SIMBIL (Position+DIP+guide)	1.63	97.93	0.060	7.04	18.48	74.30
SIMBIL (Position+DIP+guide+dilation)	1.61	98.07	0.051	5.49	17.70	77.91
Image Resolution	256 × 256					
SIMSG-CRN [6]+USR-Net [48]	14.39	95.84	0.103	18.90	28.42	77.61
SIMSG-SPADE [6]+USR-Net [48]	8.30	96.97	0.089	14.66	24.59	78.61
SIMBIL (Position+DIP)	1.85	98.16	0.069	7.13	25.38	73.48
SIMBIL (Position+DIP+guide)	1.73	98.19	0.069	8.07	19.85	75.97
SIMBIL (Position+DIP+guide+dilation)	1.71	98.30	0.061	6.55	18.86	79.48

Table 1. Quantitative results of image manipulation on CLEVR dataset. Position, DIP, guide, dilation denotes the position prediction module, deep image prior, background-guided internal learning, and mask dilation respectively.

	l_1 ↓	SSIM ↑	l_1 (RoI) ↓	SSIM(RoI) ↓
EdgeConnect [30]	1.10	98.92	29.26	66.70
Deepfillv2 [44]	1.37	98.81	39.77	65.10
SIMBIL (ours)	1.29	98.97	9.90	93.33

Table 2. Inpainting results on CLEVR. SIMBIL denotes the model with background-guided internal learning and mask dilation.

difficult to be detected by forensic detection models. Finally, qualitative examples from both CLEVR and Visual Genome are presented to demonstrate the effectiveness of our model on synthetic and natural images.

Metrics. For image manipulation, we adopt the standard image reconstruction measurements, mean absolute error (MAE), structural similarity index measure (SSIM), and perceptual metric (LPIPS) [50]. Following [6], we also report Fréchet inception distance (FID) [14] metric to assess the generated image quality. Additionally, we define the modified area of images as the Region of Interest (RoI) and report the MAE and SSIM scores. *I.e.*, RoI scores directly reflect manipulation accuracy.

For image inpainting, we adopt F_1 score to measure the correctness of the detected inpainted regions using IID-Net [40]. For each manipulated image, F_1 score is calculated in pixel level between the ground truth mask and the mask generated by detectors. We then average the F_1 score of each image to get the final result. The intuition behind this metric is that the image quality of inpaint-

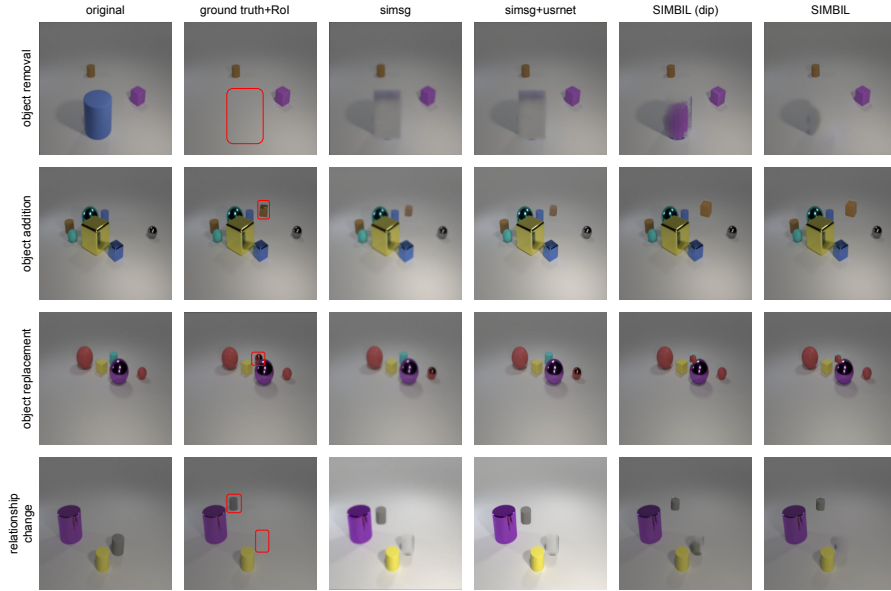


Fig. 5. Comparing SIMBIL to SIMSG-SPADE on CLEVR. The Region of Interest (RoI) is outlined by red bounding boxes. From top to bottom: object removal, object addition, object replacement, relationship change (reposition).

ing methods is likely correlated with the accuracy of an inpainting detector to identify the manipulated regions.

Baselines. For image manipulation using a scene graph, we use the code and pre-trained model weights provided by SIMSG [6] as our baseline. It has two parallel models, SIMSG-CRN and SIMSG-SPADE. Results of low resolution images (64×64 , 128×128) are directly cited from SIMSG. Note SIMSG requires more than 48GB GPU memory to train a model that outputs 256×256 images, so we apply a super-resolution network USRNet [48] on the output of SIMSG and avoid out-of-memory issues. We also adjust the code of SIMSG [6] to make the Region of Interest (RoI) metric fall within the modified regions.

For image inpainting experiments⁵, we choose two popular external learning frameworks EdgeConnect [30], Deepfillv2 [44] and an internal learning framework [37] as our baselines. The inpainting detection model is IID-Net [40], a gated convolution inpainting model that has shown high generalization ability on many inpainting methods.

⁵ In this paper, our image inpainting focuses on object removal instead of object repair.

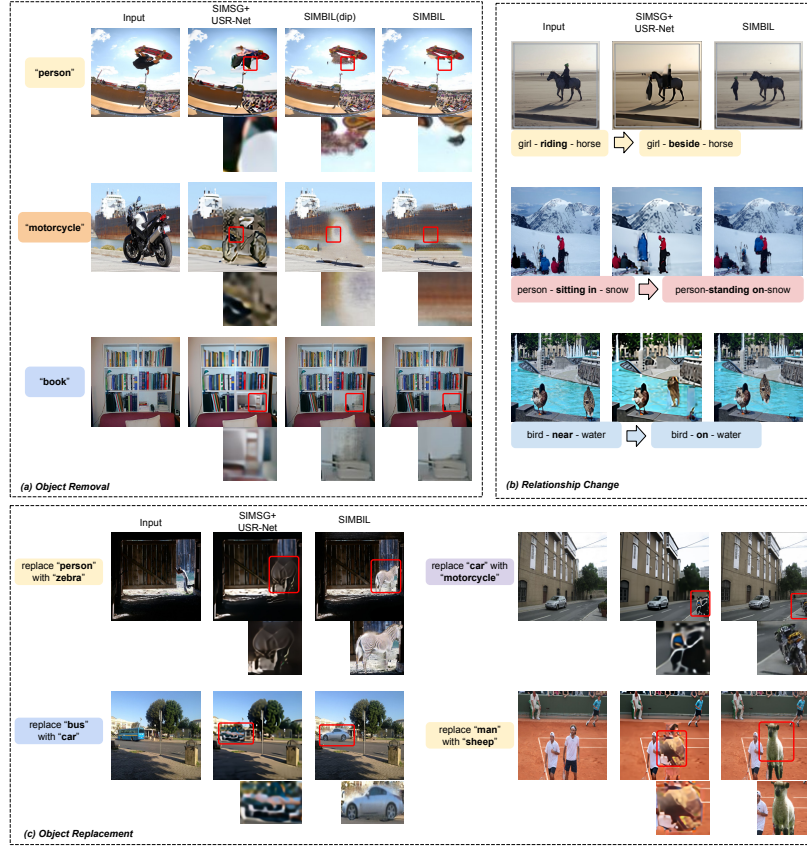


Fig. 6. Qualitative results comparing SIMBIL and SIMSG+USR-Net on Visual Genome. See Section 4.3 for discussion.

4.2 Performance on CLEVR Dataset

Manipulation Experiments. Table 1 reports quantitative results of different methods at varying image resolutions. Results of SIMSG on 64×64 and 128×128 are produced by two different models, while SIMSG+USR-Net is employed to obtain 256×256 images (for a total of four models). In contrast, SIMBIL can directly manipulate images in high resolution, *e.g.*, 256×256 , and downsample the output for results in other resolutions.

From these results, we note our base model, Position+DIP, already outperforms the baselines in “all pixels” measurements. This demonstrates the benefits of low-level manipulation, which retains the content and details of the original image. However, Position+DIP suffers from the misinformation along the boundary of missing regions as mentioned before, and harms the performance on Region of Interest (RoI). This is addressed by our approach via Position+DIP+guide and Position+DIP+guide+dilation. Specifically, Table 1 in 64×64 and 128×128

resolutions reports our Position+DIP+guide+dilation model achieves the best performance in almost all metrics. The only exception is FID, which we attribute to the fact that the distribution of the generated images can be changed by internal learning, even if this isn’t perceptible to humans. In contrast, images created by deep generative models often better match the distribution of the ground truth images. Experiments on 256×256 further validate our assumption. As shown in Table 1, even if USR-Net significantly improves image quality by human eyes, the quantitative results of SIMSG+USR-Net decrease. Thus, our model achieves the best performance across all metrics on 256×256 resolution. We provide examples for different operations in Figure 5, where SIMBIL(dip) denotes Position+DIP and SIMBIL denotes Position+DIP+guide+dilation.

Inpainting Experiments. To validate the effectiveness of background-guided internal learning on image inpainting, we compare our method with EdgeConnect [30] and Deepfill v2 [44] in Table 2, where our method outperforms both EdgeConnect and Deepfill v2, especially in the RoI.

4.3 Performance on Visual Genome Dataset

Manipulation Experiments. We generated three sets of images corresponding to object removal, object replacement, and relationship change. For each operation, we randomly selected 30 images generated by SIMSG, SIMBIL(DIP), and SIMBIL(ours) respectively (270 total). Each image is annotated three times by AMT workers and we asked our annotators to judge whether the image is correctly manipulated according to the operation. In Table 3, we report that SIMBIL(DIP) significantly outperforms SIMSG, and we achieve even higher gains with background-guided internal learning with mask dilation.

We provide qualitative results in Figure 6. Our method manipulates images on the 512×512 resolution. For comparison, we apply USR-Net to increase the resolution of SIMSG from 64×64 to 512×512 . Figure 6 (a) provides object removal examples. Similar to DeepFill v2 in Figure 3, the external approach SIMSG tends to introduce unexpected objects in some cases when inpainting. We believe the model may recognize the appearance of some objects due to seeing similar images during training. In contrast, internal learning approaches do not suffer from this issue because they only utilize the context and textures of the current input image. Additionally, our background-guided method provides higher quality images compared to DIP. Figure 6 (b) presents images reports by a relationship change. From these results, we can see that our position prediction module outputs reasonable values for the relationship change between objects, for instance, riding \rightarrow beside, sitting in \rightarrow standing on, near \rightarrow on. Finally, Figure 6 (c) provides object replacement results, where we clearly outperform SIMSG-generated images. See the supplementary for additional results and comparisons.

Inpainting Experiments. Table 4 compares different inpainting methods on Visual Genome. As we discussed in Section 4.1, we use an inpainting detector IID-Net to predict where the images have been manipulated and report the F_1

	Object Removal	Object Replacement	Relationship Change
SIMSG+USR-Net	17.8%	24.4 %	15.6%
SIMBIL(DIP)	32.3%	35.6%	35.6%
SIMBIL(ours)	50.0%	40.0%	48.9%

Table 3. User evaluation of image manipulation on Visual Genome. See Section 4.3 for discussion.

	$F_1 \downarrow$ User Evaluation \uparrow	
EdgeConnect [30]	33.5	12.2%
Deepfillv2 [44]	33.8	13.3%
DIP [37]	8.7	25.6%
SIMBIL(ours)	7.1	48.9%

Table 4. Quantitative comparison of image inpainting on Visual Genome, using F_1 score detected by IID-Net [40] and user evaluation as metrics. See Section 4.3 for discussion.

score since Visual Genome lacks ground truth edited images. Note lower is better since that means the manipulations are harder to detect.

For human evaluation, we also use the same experiment settings to our manipulation experiments, *i.e.*, we selected 30 images for each model and each image is annotated three times. We presented each worker with images generated by EdgeConnect [30], Deepfillv2 [44], DIP [37], SIMBIL respectively. The users were asked to choose the image with inpainting highest quality. From the table, we see that the internal learning methods, DIP and SIMBIL significantly outperform the external learning methods, EdgeConnect and Deepfillv2, supporting our analysis in Section 3.3. Though the DIP achieves comparable performance with SIMBIL on F_1 score, we observe that users significantly prefer the SIMBIL-generated images, demonstrating the effectiveness of our proposed background-guided internal learning.

4.4 Limitations and Future Work

In this section, we analyze the limitations of our method and provide suggestions to address these limitations. Four cases are provided in Figure 7.

- (a) **Shadow removal:** Since Mask R-CNN does not consider shadows as part of an object, they typically remain in an image. However, this can be addressed by incorporating shadow detection methods (*e.g.*, [38]) in the removal module.
- (b) **Artificial boundary:** In some images, we can observe white edges if we zoom out the boundary region of the modified object. We assume the artificial boundary is introduced when we resize the object from the query images.
- (c) **Biased background:** Although background-guided internal learning outperforms DIP in most cases, we do have some failures like the example in Figure 7(c). We believe this is because Mask R-CNN is pre-trained on COCO and can

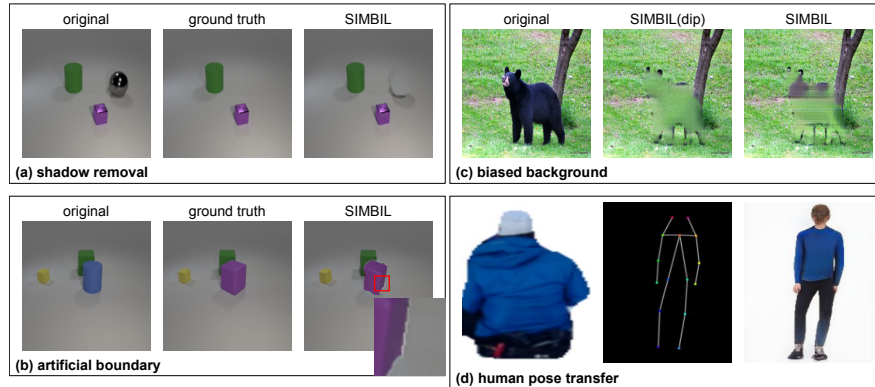


Fig. 7. Limitations of SIMBIL. See Section 4.4 for discussion.

not distinguish the tree from the background. As a result, our approach guides the missing region to be similar to the tree in some areas within the “hole”.

(d) **Human pose transfer:** Relationships between objects are not limited to spatial relationships such as beside, near, on, but also span predicates like standing on, running, walking. Ideally, the appearance of the objects should also be changed according to various predicates. We tried to apply a human pose transfer model [57] pretrained on DeepFashion [28] to address this issue. However, there is a significant domain shift from DeepFashion to Visual Genome that resulted in poor performance, which could be addressed in future work via domain adaptation techniques.

(e) **Inference time:** Internal learning methods train a separate network to process each image. The inference time to process a 512×512 image by a RTX 3090 takes approximately 160 seconds. However, we observe that our background-guidance mechanism has negligible overhead compared to DIP.

5 Conclusion

In this paper, we proposed a semantic image manipulation method called SIMBIL that combines high-level image semantics with low-level manipulation. SIMBIL mainly consists of three modules: object removal module via Mask R-CNN, an RNN-based module to predict the new position of the target object, and a background-guided internal learning module for image inpainting. SIMBIL outperforms the state-of-the-art in a qualitative and quantitative evaluation on CLEVR and Visual Genome datasets. Extensive experiments on images with higher resolution, which prior work struggled to perform, further demonstrate the effectiveness of our method. Thus, we argue the combination of high-level semantics and low-level manipulation is a promising way to solve the image manipulation problem since it requires less human effort and accurately preserves the original image’s attributes and details.

Acknowledgements. This work was supported in part by DARPA under agreement number HR00112020054.

References

1. Bau, D., Strobel, H., Peebles, W., Zhou, B., Zhu, J.Y., Torralba, A., et al.: Semantic photo manipulation with a generative image prior. arXiv preprint arXiv:2005.07727 (2020)
2. Brock, A., Lim, T., Ritchie, J.M., Weston, N.: Neural photo editing with introspective adversarial networks. arXiv preprint arXiv:1609.07093 (2016)
3. Chan, C., Ginosar, S., Zhou, T., Efros, A.A.: Everybody dance now. In: Proceedings of the IEEE/CVF International Conference on Computer Vision. pp. 5933–5942 (2019)
4. Choi, Y., Choi, M., Kim, M., Ha, J.W., Kim, S., Choo, J.: Stargan: Unified generative adversarial networks for multi-domain image-to-image translation. In: Proceedings of the IEEE conference on computer vision and pattern recognition. pp. 8789–8797 (2018)
5. Dai, B., Zhang, Y., Lin, D.: Detecting visual relationships with deep relational networks. In: Proceedings of the IEEE conference on computer vision and Pattern recognition. pp. 3076–3086 (2017)
6. Dhama, H., Farshad, A., Laina, I., Navab, N., Hager, G.D., Tombari, F., Rupprecht, C.: Semantic image manipulation using scene graphs. In: Proceedings of the IEEE/CVF Conference on Computer Vision and Pattern Recognition. pp. 5213–5222 (2020)
7. El-Nouby, A., Sharma, S., Schulz, H., Hjelm, D., Asri, L.E., Kahou, S.E., Bengio, Y., Taylor, G.W.: Tell, draw, and repeat: Generating and modifying images based on continual linguistic instruction. In: Proceedings of the IEEE/CVF International Conference on Computer Vision. pp. 10304–10312 (2019)
8. Gandelsman, Y., Shocher, A., Irani, M.: ” double-dip”: Unsupervised image decomposition via coupled deep-image-priors. In: Proceedings of the IEEE/CVF Conference on Computer Vision and Pattern Recognition. pp. 11026–11035 (2019)
9. Gatys, L.A., Ecker, A.S., Bethge, M.: Image style transfer using convolutional neural networks. In: Proceedings of the IEEE conference on computer vision and pattern recognition. pp. 2414–2423 (2016)
10. Goodfellow, I., Pouget-Abadie, J., Mirza, M., Xu, B., Warde-Farley, D., Ozair, S., Courville, A., Bengio, Y.: Generative adversarial nets. *Advances in neural information processing systems* **27** (2014)
11. Guasch, L., Agudo, O.C., Tang, M.X., Nachev, P., Warner, M.: Full-waveform inversion imaging of the human brain. *NPJ digital medicine* **3**(1), 1–12 (2020)
12. He, K., Gkioxari, G., Dollár, P., Girshick, R.: Mask r-cnn. In: Proceedings of the IEEE international conference on computer vision. pp. 2961–2969 (2017)
13. Herzig, R., Raboh, M., Chechik, G., Berant, J., Globerson, A.: Mapping images to scene graphs with permutation-invariant structured prediction. arXiv preprint arXiv:1802.05451 (2018)
14. Heusel, M., Ramsauer, H., Unterthiner, T., Nessler, B., Hochreiter, S.: Gans trained by a two time-scale update rule converge to a local nash equilibrium. arXiv preprint arXiv:1706.08500 (2017)
15. Hu, R., Dollár, P., He, K., Darrell, T., Girshick, R.: Learning to segment every thing. In: Proceedings of the IEEE Conference on Computer Vision and Pattern Recognition. pp. 4233–4241 (2018)

16. Hu, R., Rohrbach, M., Darrell, T.: Segmentation from natural language expressions. In: The European Conference on Computer Vision (ECCV) (2016)
17. Jo, Y., Park, J.: Sc-fegan: face editing generative adversarial network with user's sketch and color. In: Proceedings of the IEEE/CVF International Conference on Computer Vision. pp. 1745–1753 (2019)
18. Johnson, J., Hariharan, B., Van Der Maaten, L., Fei-Fei, L., Lawrence Zitnick, C., Girshick, R.: Clevr: A diagnostic dataset for compositional language and elementary visual reasoning. In: Proceedings of the IEEE Conference on Computer Vision and Pattern Recognition. pp. 2901–2910 (2017)
19. Johnson, J., Krishna, R., Stark, M., Li, L.J., Shamma, D., Bernstein, M., Fei-Fei, L.: Image retrieval using scene graphs. In: Proceedings of the IEEE conference on computer vision and pattern recognition. pp. 3668–3678 (2015)
20. Krishna, R., Chami, I., Bernstein, M., Fei-Fei, L.: Referring relationships. In: Proceedings of the IEEE Conference on Computer Vision and Pattern Recognition. pp. 6867–6876 (2018)
21. Krishna, R., Zhu, Y., Groth, O., Johnson, J., Hata, K., Kravitz, J., Chen, S., Kalantidis, Y., Li, L.J., Shamma, D.A., et al.: Visual genome: Connecting language and vision using crowdsourced dense image annotations. *International journal of computer vision* **123**(1), 32–73 (2017)
22. Lee, C.H., Liu, Z., Wu, L., Luo, P.: Maskgan: Towards diverse and interactive facial image manipulation. In: Proceedings of the IEEE/CVF Conference on Computer Vision and Pattern Recognition. pp. 5549–5558 (2020)
23. Li, B., Qi, X., Lukasiewicz, T., Torr, P.H.: Manigan: Text-guided image manipulation. In: Proceedings of the IEEE/CVF Conference on Computer Vision and Pattern Recognition. pp. 7880–7889 (2020)
24. Li, Y., Ouyang, W., Zhou, B., Shi, J., Zhang, C., Wang, X.: Factorizable net: an efficient subgraph-based framework for scene graph generation. In: Proceedings of the European Conference on Computer Vision (ECCV). pp. 335–351 (2018)
25. Li, Y., Ouyang, W., Zhou, B., Wang, K., Wang, X.: Scene graph generation from objects, phrases and region captions. In: Proceedings of the IEEE International Conference on Computer Vision. pp. 1261–1270 (2017)
26. Liang, X., Zhang, H., Lin, L., Xing, E.: Generative semantic manipulation with mask-contrasting gan. In: Proceedings of the European Conference on Computer Vision (ECCV). pp. 558–573 (2018)
27. Lin, T.Y., Maire, M., Belongie, S., Hays, J., Perona, P., Ramanan, D., Dollár, P., Zitnick, C.L.: Microsoft coco: Common objects in context. In: European conference on computer vision. pp. 740–755. Springer (2014)
28. Liu, Z., Luo, P., Qiu, S., Wang, X., Tang, X.: Deepfashion: Powering robust clothes recognition and retrieval with rich annotations. In: Proceedings of the IEEE conference on computer vision and pattern recognition. pp. 1096–1104 (2016)
29. Lu, C., Krishna, R., Bernstein, M., Fei-Fei, L.: Visual relationship detection with language priors. In: European conference on computer vision. pp. 852–869. Springer (2016)
30. Nazeri, K., Ng, E., Joseph, T., Qureshi, F., Ebrahimi, M.: Edgeconnect: Structure guided image inpainting using edge prediction. In: Proceedings of the IEEE/CVF International Conference on Computer Vision Workshops. pp. 0–0 (2019)
31. Plummer, B.A., Mallya, A., Cervantes, C.M., Hockenmaier, J., Lazebnik, S.: Phrase localization and visual relationship detection with comprehensive image-language cues. In: Proceedings of the IEEE International Conference on Computer Vision. pp. 1928–1937 (2017)

32. Plummer, B.A., Shih, K., Li, Y., Xu, K., Lazebnik, S., Sclaroff, S., Saenko, K.: Revisiting image-language networks for open-ended phrase detection. *IEEE Transactions on Pattern Analysis and Machine Intelligence* (2020)
33. Qi, M., Li, W., Yang, Z., Wang, Y., Luo, J.: Attentive relational networks for mapping images to scene graphs. In: *Proceedings of the IEEE/CVF Conference on Computer Vision and Pattern Recognition*. pp. 3957–3966 (2019)
34. Ren, S., He, K., Girshick, R., Sun, J.: Faster r-cnn: Towards real-time object detection with region proposal networks. *arXiv preprint arXiv:1506.01497* (2015)
35. Shetty, R., Fritz, M., Schiele, B.: Adversarial scene editing: Automatic object removal from weak supervision. *arXiv preprint arXiv:1806.01911* (2018)
36. Teterwak, P., Sarna, A., Krishnan, D., Maschinot, A., Belanger, D., Liu, C., Freeman, W.T.: Boundless: Generative adversarial networks for image extension. In: *Proceedings of the IEEE/CVF International Conference on Computer Vision*. pp. 10521–10530 (2019)
37. Ulyanov, D., Vedaldi, A., Lempitsky, V.: Deep image prior. In: *Proceedings of the IEEE conference on computer vision and pattern recognition*. pp. 9446–9454 (2018)
38. Wang, T., Hu, X., Wang, Q., Heng, P.A., Fu, C.W.: Instance shadow detection. In: *Proceedings of the IEEE/CVF Conference on Computer Vision and Pattern Recognition*. pp. 1880–1889 (2020)
39. Wang, T.C., Liu, M.Y., Zhu, J.Y., Tao, A., Kautz, J., Catanzaro, B.: High-resolution image synthesis and semantic manipulation with conditional gans. In: *Proceedings of the IEEE conference on computer vision and pattern recognition*. pp. 8798–8807 (2018)
40. Wu, H., Zhou, J.: Iid-net: Image inpainting detection network via neural architecture search and attention. *IEEE Transactions on Circuits and Systems for Video Technology* pp. 1–1 (2021). <https://doi.org/10.1109/TCSVT.2021.3075039>
41. Xu, D., Zhu, Y., Choy, C.B., Fei-Fei, L.: Scene graph generation by iterative message passing. In: *Proceedings of the IEEE conference on computer vision and pattern recognition*. pp. 5410–5419 (2017)
42. Yang, J., Lu, J., Lee, S., Batra, D., Parikh, D.: Graph r-cnn for scene graph generation. In: *Proceedings of the European conference on computer vision (ECCV)*. pp. 670–685 (2018)
43. Yeh, R.A., Chen, C., Yian Lim, T., Schwing, A.G., Hasegawa-Johnson, M., Do, M.N.: Semantic image inpainting with deep generative models. In: *Proceedings of the IEEE conference on computer vision and pattern recognition*. pp. 5485–5493 (2017)
44. Yu, J., Lin, Z., Yang, J., Shen, X., Lu, X., Huang, T.S.: Free-form image inpainting with gated convolution. In: *Proceedings of the IEEE/CVF International Conference on Computer Vision*. pp. 4471–4480 (2019)
45. Zellers, R., Yatskar, M., Thomson, S., Choi, Y.: Neural motifs: Scene graph parsing with global context. In: *Proceedings of the IEEE Conference on Computer Vision and Pattern Recognition*. pp. 5831–5840 (2018)
46. Zeng, Y., Fu, J., Chao, H., Guo, B.: Learning pyramid-context encoder network for high-quality image inpainting. In: *Proceedings of the IEEE/CVF Conference on Computer Vision and Pattern Recognition*. pp. 1486–1494 (2019)
47. Zhang, H., Mai, L., Xu, N., Wang, Z., Collomosse, J., Jin, H.: An internal learning approach to video inpainting. In: *Proceedings of the IEEE/CVF International Conference on Computer Vision*. pp. 2720–2729 (2019)
48. Zhang, K., Gool, L.V., Timofte, R.: Deep unfolding network for image super-resolution. In: *Proceedings of the IEEE/CVF Conference on Computer Vision and Pattern Recognition*. pp. 3217–3226 (2020)

49. Zhang, R., Isola, P., Efros, A.A.: Colorful image colorization. In: European conference on computer vision. pp. 649–666. Springer (2016)
50. Zhang, R., Isola, P., Efros, A.A., Shechtman, E., Wang, O.: The unreasonable effectiveness of deep features as a perceptual metric. In: Proceedings of the IEEE conference on computer vision and pattern recognition. pp. 586–595 (2018)
51. Zhang, Z., Lin, Y.: Data-driven seismic waveform inversion: A study on the robustness and generalization. *IEEE Transactions on Geoscience and Remote sensing* **58**(10), 6900–6913 (2020)
52. Zhang, Z., Wu, Y., Zhou, Z., Lin, Y.: Velocitygan: Subsurface velocity image estimation using conditional adversarial networks. In: 2019 IEEE Winter Conference on Applications of Computer Vision (WACV). pp. 705–714. IEEE (2019)
53. Zhao, B., Chang, B., Jie, Z., Sigal, L.: Modular generative adversarial networks. In: Proceedings of the European conference on computer vision (ECCV). pp. 150–165 (2018)
54. Zhao, Y., Price, B., Cohen, S., Gurari, D.: Guided image inpainting: Replacing an image region by pulling content from another image. In: 2019 IEEE Winter Conference on Applications of Computer Vision (WACV). pp. 1514–1523. IEEE (2019)
55. Zhou, B., Lapedriza, A., Khosla, A., Oliva, A., Torralba, A.: Places: A 10 million image database for scene recognition. *IEEE transactions on pattern analysis and machine intelligence* **40**(6), 1452–1464 (2017)
56. Zhu, J.Y., Krähenbühl, P., Shechtman, E., Efros, A.A.: Generative visual manipulation on the natural image manifold. In: European conference on computer vision. pp. 597–613. Springer (2016)
57. Zhu, Z., Huang, T., Shi, B., Yu, M., Wang, B., Bai, X.: Progressive pose attention transfer for person image generation. In: Proceedings of the IEEE/CVF Conference on Computer Vision and Pattern Recognition. pp. 2347–2356 (2019)

Appendices

A Implementation Details

A.1 Mask R-CNN

CLEVR. We apply the CLEVR framework [18] to generate a dataset consisting of 1,000 images with object masks. Following [6], Mask R-CNN is trained to classify the objects into 24 categories with 3 shapes (sphere, cylinder, cube) and 8 colors (blue, yellow, purple, green, red, gray, cyan, brown).

Visual Genome. We directly use the Mask R-CNN model pre-trained on COCO [27] for Visual Genome. In this paper, we focus on objects that the Mask R-CNN is trained to identify. However, these categories can be greatly expanded using methods like the transfer learning approach Mask^X R-CNN [15] or segmenting entities based on natural language queries [16].

A.2 Position Prediction

CLEVR. As we mentioned in the main paper, the modified triplets, bounding boxes of reference objects and target objects are extracted from 6,688 images

as our training data. 818 images are adopted as the validation set. We set the maximum number of the modified triplets of each image to 5. The mean absolute error (mae) on validation set is 12.05 ± 0.87 (computed over 5 runs), where the image size is 256×256 . It should be mentioned that the gap between the predicted value and ground truth value does not necessarily indicate the predicted value is incorrect. Any points in the correct region can satisfy the relationships between objects. For instance, if a blue cube is on the right side of a red sphere, then any positions on the right side of the red sphere should be correct. Therefore, the accuracy of our model is underreported.

Visual Genome. Similar to CLEVR, we use 40,000 images for training and 2089 images for evaluation. The mae on validation set is 77.84 ± 1.25 (computed over 5 runs), where the image size is 512×512 .

A.3 Background-guided Internal Learning

We use the encoder-decoder structure with skip connections [37] for our inpainting model. The iteration number for each image is set to 2,000 and λ in Eq. 5 is set to 0.1. For CLEVR, we constrain the average of each missing region by a single value. For Visual Genome, we constrain the average of missing regions row by row.

B Additional Experiments

Additional Qualitative Results. Figures 8, 9, & 10 provide additional qualitative results that demonstrating SIMBIL outperforms prior work on Visual Genome to supplement the results from the main paper.

Ablation Study. Table 5 provides the ablation study of mask dilation, validating that the improvements of SIMBIL are based on both the background-guided mechanism and the mask dilation.

Method	All pixels				RoI only	
	MAE ↓	SSIM ↑	LPIPS ↓	FID ↓	MAE ↓	SSIM ↑
Position+DIP	1.85	98.16	0.069	7.13	25.38	73.48
Position+DIP+guide	1.73	98.19	0.069	8.07	19.85	75.97
Position+DIP+dilation	1.72	98.26	0.065	7.21	22.02	75.60
Position+DIP+guide+dilation	1.71	98.30	0.061	6.55	18.86	79.48

Table 5. Ablation study of mask dilation on CLEVR (256×256 image).

Diverse Outputs. As we discussed in Section A.2, a modified scene graph can point to different outputs with correct semantics based on the same input. We generate diverse outputs using the manipulated relationship’s probability map shown in Figure 11.

Semantic correctness of edits. To illustrate that the incorrect semantics of manipulated images could be captured by our quantitative metrics in the main paper, we performed a comparison experiment in Table 6. We applied modified scene graph A and modified scene graph B on the same input and compared their outputs with the ground truth label of scene graph A (note $A \neq B$). We see the correctly modified image has significantly better results.

	l_1 (RoI) ↓	SSIM(RoI) ↑		l_1 (RoI) ↓	SSIM(RoI) ↑
A	18.86	79.48	B	41.04	65.56

Table 6. Comparison of evaluating modifications A and B. See **Semantic correctness of edits** of Section B for details.

Iterations in optimization. We compare the iterations of DIP and SIMBIL in Figure 12 to demonstrate the improvement of our background-guided mechanism. *E.g.*, in the bottom figure, the removed object is blue cylinder and DIP uses the color of purple cube which is far from the blue cylinder to fill in the missing part. In contrast, SIMBIL uses the color of grey background to fill in the missing part.

C Defending against Machine-manipulated Images

In our paper, we develop a model called SIMBIL for both semantic image manipulation and image inpainting. From the experiments, we see that SIMBIL not only generates higher-quality images (according to quantitative experiments and human assessments) but also be much more difficult to be recognized and located by existing image manipulation detection methods like IIDNet [40]. This can be due to the fact that most existing detection models are trained on images generated by external learning methods like Deepfill [44] or EdgeConnect [30]. Thus, our internal learning method also provides a potential improvement direction for image manipulation detection, *i.e.*, how to develop a more robust framework that can recognize both the external learning manipulated images and the internal learning manipulated images.

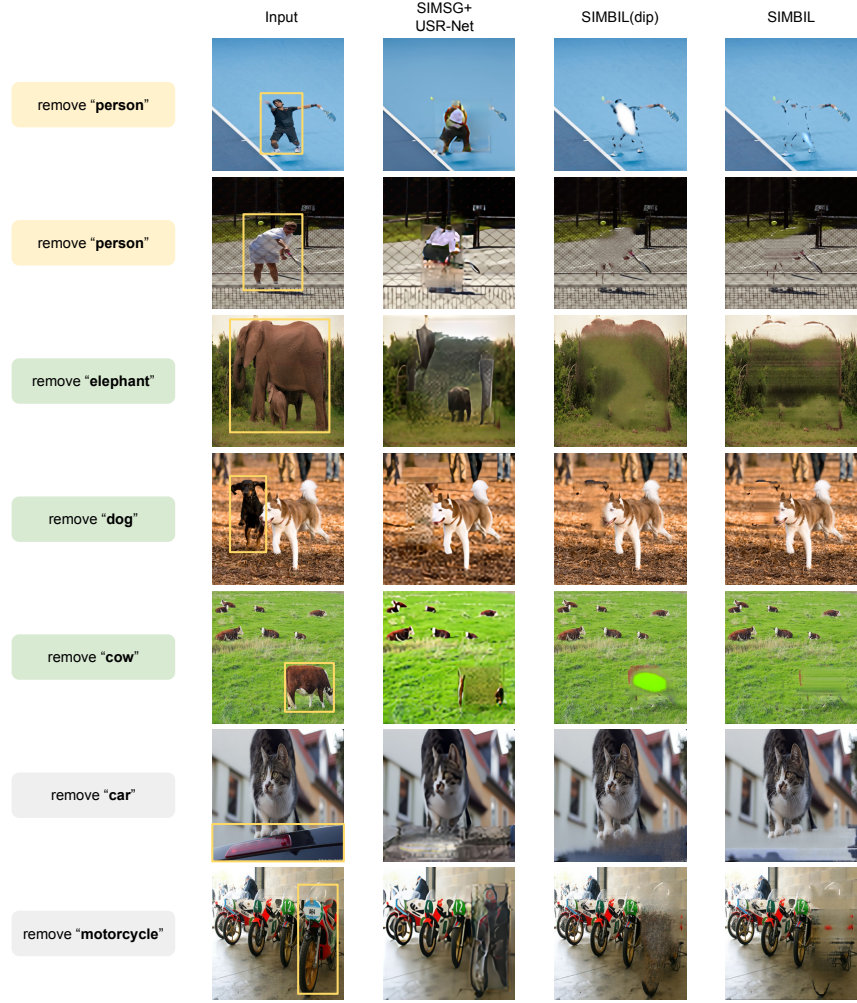


Fig. 8. Object Removal. Target objects are outlined by light yellow bounding boxes

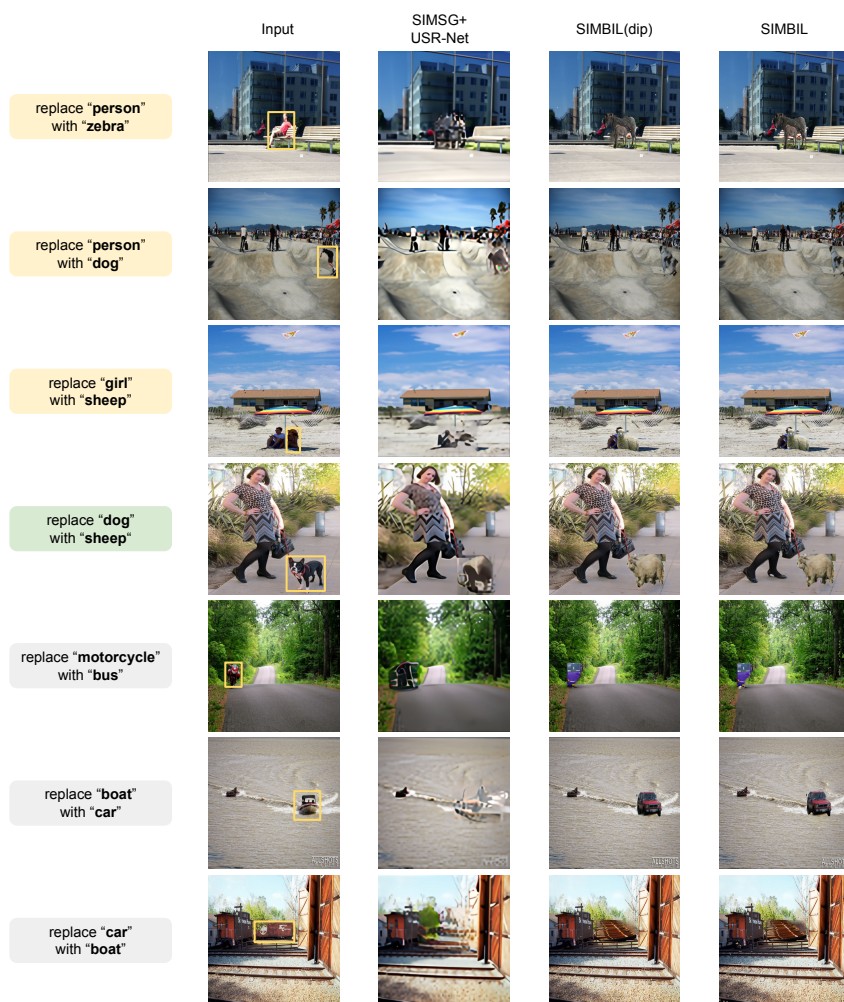


Fig. 9. Object Replacement.

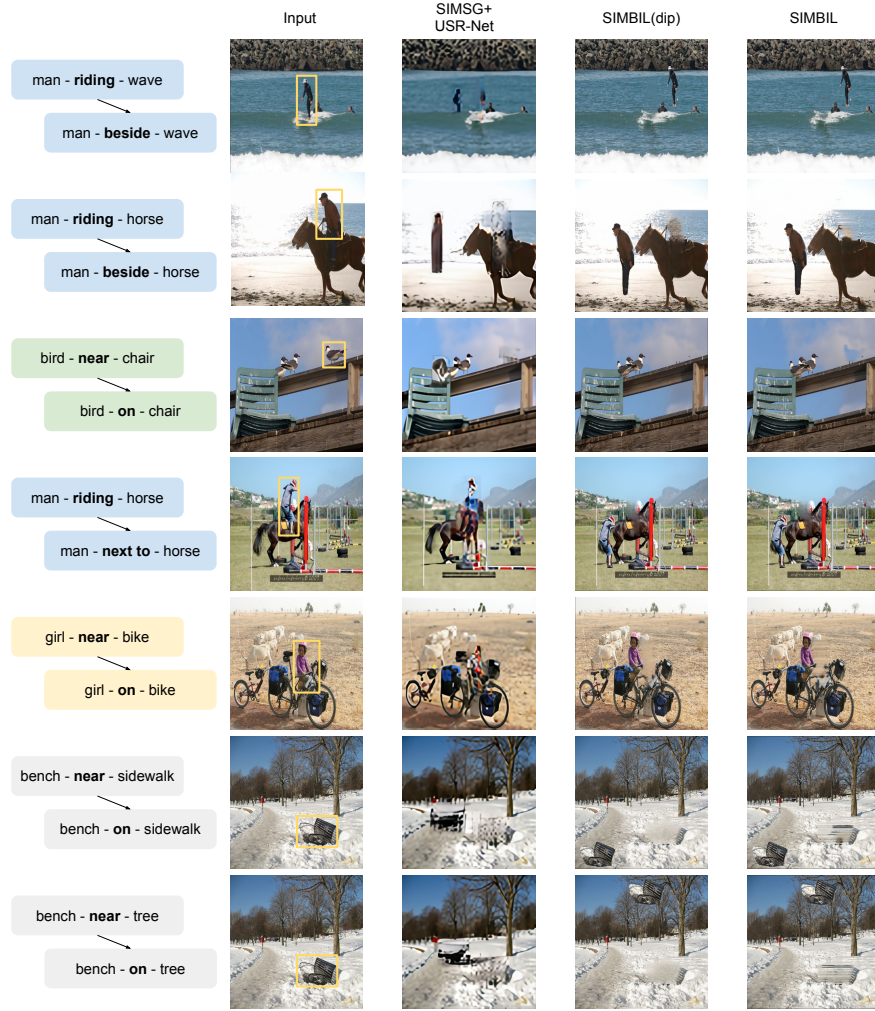


Fig. 10. Relationship Change

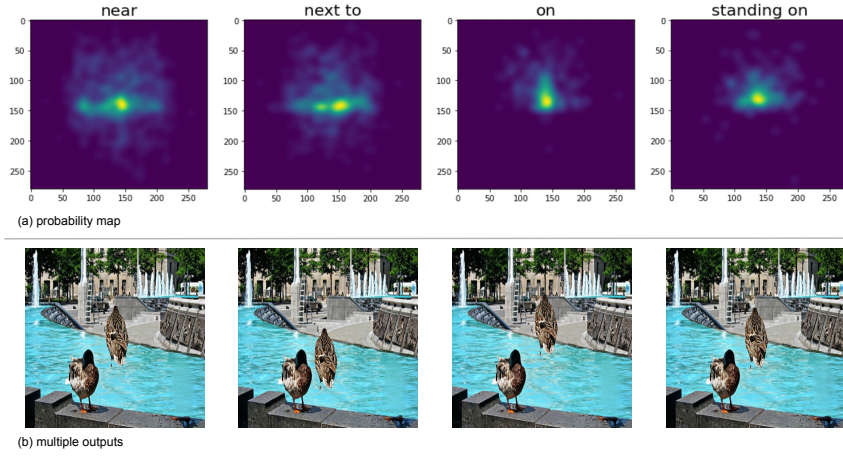


Fig. 11. Top: probability map of selected predicates; Bottom: an example of diverse outputs, “bird-on-water”.

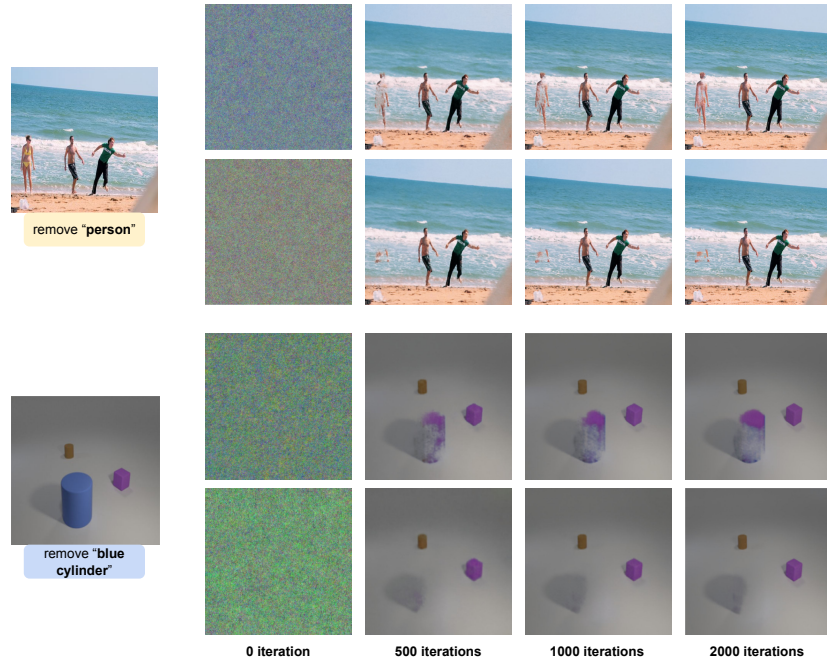


Fig. 12. The iterations of Deep Image Prior [37] (top row of each image) and our method (bottom row of each image). We use background-guided mechanism to constrain the optimization of deep image prior and generate plausible results.